Intelligent Approach for PET Volume Analysis

Mhd Saeed Sharif, Abbes Amira
School of Engineering and Design
Brunel University, West London, United Kingdom
mhd.sharif@brunel.ac.uk

Habib Zaidi
Division of Nuclear Medicine
Geneva University Hospital
CH-1211 Geneva, Switzerland

***Abstract*—Tumour classification and quantification in positron emission tomography (PET) imaging at early stage of illness are important for radiotherapy planning, tumour diagnosis, and fast recovery. Analysing large medical volumes using traditional techniques requires a decent amount of time, and in some approaches poor accuracy is achieved. Artificial intelligence (AI) technologies can provide better accuracy and save decent amount of time. Artificial neural network (ANN), as one of the best AI technologies, has the capability to classify, measure precisely the region of interest, and model the clinical evaluation for a specific problem. This paper presents a novel application of the ANN in the wavelet domain for PET volume segmentation. ANN performance evaluation using different number of hidden neurons is also considered. The proposed intelligent system outputs are compared with the outputs of thresholding, and clustering based approaches. Two PET phantom data sets and real PET volumes have been utilised to validate the proposed system which has shown promising results.**

I. Introduction

PET is a tomographic technique which is used to measure physiology and function rather than anatomy by imaging elements such as carbon, oxygen and nitrogen which have a high abundance within human body. Among all diagnostic and therapeutic procedures, PET is unique in the sense that it is based on molecular and pathophysiological mechanisms and employs radioactively labeled biological molecules as tracers to study the pathophysiology of the tumour in vivo to direct treatment and assess response to therapy. The leading current area of clinical use of PET is in oncology, where ^{18}F-fluorodeoxyglucose (FDG) remains the most widely used tracer. It has already had a large valuable effect on cancer staging and treatment and its use in clinical oncology practice continues to evolve [1] [2].

The main expected challenge of PET modality is the low resolution which is known as a spatial volume effect. This effect should be reduced to the minimum level, so the required information can be precisely extracted from the analysed volume. The increasing number of scans beside the widespread application of PET modality have increased the urgent need for effective volume analysis techniques to aid clinicians in tumour diagnosis and put the proper plan for treatment. Analysing and extracting the proper information from PET volumes can be performed by utilising segmentation and classification approaches which provide richer information than that which exists in the original PET volumes alone. The need for accurate and fast analysis for medical volume segmentation leads to exploit AI technologies.

ANN is one of the powerful AI techniques that has the capability to learn a set of data and construct weight matrices to represent the learning patterns. The ANN is a mathematical model which emulates the activity of biological neural networks in the human brain. It consists of two or several layers each one has many interconnected groups of neurons. ANN has great success in many applications including pattern classification, decision making, forecasting, and adaptive control. Many research studies have been carried out in the medical field utilising ANN for medical image segmentation and classification with different medical image modalities [3] [4].

The main aim of this paper is to develop a robust efficient PET volume segmentation system using ANN. ANN performance has been measured using different performance metrics. ANN outputs are compared with the outputs of thresholding and clustering based approaches.

This paper is organised as follows. Section II presents mathematical background for the selected approaches. The proposed medical volume segmentation system is described in section III. Experimental results and analysis are illustrated in section IV, and finally conclusions and future work are presented in section V.

II. Mathematical Background

A. Mathematical model of a neuron

Each neuron in the ANN has a number of inputs (P) and one output (Y). The input vector elements are multiplied by weights $w_{1,1}$, $w_{1,2}$, ... , $w_{1,R}$, and the weighted values are fed to the summing junction. Their sum is simply the dot product ($W.P$) of the single row matrix W and the vector P. The neuron has a bias b, which is summed with the weighted inputs to form the net input n. This sum, n, is the argument of the transfer function f [5].

$$n = \sum_{i=1}^{R} w_{1,i}.p_i + b \tag{1}$$

$$Y = f(W.P + b) \tag{2}$$

$$Y(j) = f[\sum_{i=1}^{R} w_{1,i}(j).p_i(j) + b] \tag{3}$$

The learning process can be summarized in the following steps: 1) the initial weights are randomly assigned, 2) the neuron is activated by applying inputs vector and desired output (Y_d), and 3) calculation of the actual output (Y) at iteration j=1 as illustrated in Eq. 3, where iteration j refers to the jth training example presented to the neuron. The following step is to update the weights to obtain an output consistent with the training examples, as illustrated in Eq. 4.

$$w_{1,i}(j+1) = w_{1,i}(j) + \Delta w_{1,i}(j) \tag{4}$$

where $\Delta w_{1,i}(j)$ is the weight correction at iteration j. The weight correction is computed by using the delta rule in Eq. 5

$$\Delta w_{1,i}(j) = \alpha * p_i(j) * e(j) \tag{5}$$

where α is the learning rate and $e(j)$ is the error which can be given by Eq. 6

$$e(j) = Y_d(j) - Y(j) \tag{6}$$

Finally, the iteration j is increased by one, and the previous two steps are repeated until the convergence is reached.

978-1-4244-5309-2/10/$26.00 ©2010 IEEE

B. Thresholding

1) Hard Thresholding: This methodology attempts to determine an intensity value that can separate the volume into two parts [6]. All voxels with intensities *f(x,y)* larger than the threshold value *T* are allocated into one class, and all the others into another class. Thresholding approach does not consider the spatial characteristics of the volume; it is sensitive to noise and intensities variation.

2) Soft Thresholding: This approach replaces each voxel which has a greater value than the threshold value by the difference between the threshold and the voxel values. Soft thresholding can illustrate some important regions as the region of interest (ROI) in this study.

3) Adaptive thresholding: Otsu's method has been used as a third approach, which chooses the threshold that minimizes the intraclass variance of the black and white voxels in the volume [7].

C. Multiresolution analysis

Multiresolution analysis (MRA) is designed to give good time resolution and poor frequency resolution at high frequencies, and poor time resolution and good frequency resolution at low frequencies. It enables the exploitation of slice characteristics associated with a particular resolution level, which may not be detected using other analysis techniques [8] [9]. The wavelet transform for a function *f(t)* can be defined as follow:

$$X_{\psi_{(a,b)}} = \int_{-\infty}^{\infty} f(t)\psi_{(a,b)}(t)dt \tag{7}$$

where

$$\psi_{(a,b)}(t) = \frac{1}{\sqrt{a}}\psi(\frac{t-b}{a}) \tag{8}$$

The parameters *a, b* are called the scaling and shifting parameters, respectively [8] [10]. Haar wavelet filter will be used in the experimental study at different levels of decomposition. Haar wavelet transform (HWT) of a two-dimensional slice can be performed using two approaches: the first one is called standard decomposition where the one-dimensional HWT is applied to each row of pixel values followed by another one-dimensional HWT on the column of the processed slice. The other approach is called non-standard decomposition, which alternates between the one-dimensional HWT operations on rows and columns. HWT is conceptually simple, fast, memory efficient, and it can be reversed without the edge effects that are associated with other wavelet transforms.

D. Clustering

Clustering technique is aiming to classify each voxel in a volume into the proper cluster, then these clusters are mapped to display the segmented volume. The most commonly used clustering technique is the *K*-means method, which clusters *n* voxels into *K* clusters (*K* less than *n*) [11]. This algorithm chooses the number of clusters, *K*, then randomly generates *K* clusters and determines the cluster centers. The next step is assigning each voxel in the volume to the nearest cluster center, and finally recompute the new cluster centers. The two previous steps are repeated until the minimum variance criterion is achieved. The main approach objective is to achieve a minimum intra-cluster variance *V*.

$$V = \sum_{i=1}^{K} \sum_{x_j \in S_i} (x_j - \mu_i)^2 \tag{9}$$

where *K* is the number of clusters, *S=1,2,...K*, and the mean of all voxels in cluster *i* is μ_i.

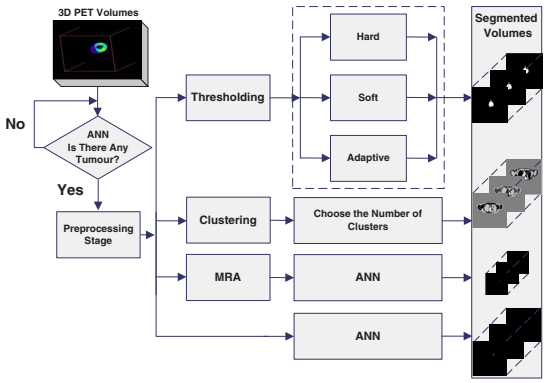

Fig. 1. Proposed system for PET volume segmentation.

III. THE PROPOSED SYSTEM

The proposed medical volume segmentation system is illustrated in Fig. 1. The 3D PET volume acquired from the scanner goes through the checking block, where ANN is used to check each slice from the volume, if the slice contains the ROI then it proceeds to the preprocessing stage. At this stage histogram equalisation and median filter are utilised to enhance the quality of slices features and remove most of the noise in each slice. The enhanced volume can be processed using three approaches, the first one is the thresholding which removes the background and unnecessary information producing a volume which consists of two classes the background and the ROI. The second approach is *K*-means clustering technique which classifies PET volume into an appropriate number of clusters. The third approach is ANN which is used in spatial and wavelet domains. The preprocessed PET volume is fed first to ANN which is trained to detect tumour. In another block PET volume is transformed into the wavelet domain using HWT at different levels of decomposition. HWT decomposes the volume and produces the approximation, horizontal, vertical, and diagonal features for each slice. The approximation features are fed to another ANN for detecting and quantifying the tumour. The outputs of ANNs are compared in the next step with the outputs of the other two approaches, while the best outputs are selected and displayed.

IV. EXPERIMENTAL RESULTS AND ANALYSIS

A. Studying PET phantom data

In this study, PET volumes containing simulated tumour have been utilised. Two phantom data sets have been used, the first data set is obtained from NEMA IEC image quality body phantom which consists of an elliptical water filled cavity with six spherical inserts suspended by plastic rods of volumes 0.5, 1.2, 2.6, 5.6, 11.5, and 26.5 ml. The inner diameters of these spheres are: 10, 13, 17, 22, 28 and 37 mm. The scanner used for acquiring this volume has a resolution of 4.07 mm x 4.07 mm x 5 mm, with voxel volume 0.0828 ml, while the size of the obtained phantom volume is 168 x 168 x 66. The second data set is Zubal phantom volume, which were simulated using a validated PET Monte Carlo simulation package [12]. The volume contains a raw matrix with isotropic voxels, the size of this volume is 128 x 128 x 180, and the voxel size is 5.0625 mm x 5.0625 mm x 2.4250 mm. The second data volumes have 3 tumours in the lungs as follows: tumour 1 is allocated in slice 68, tumour 2 is allocated in slice 57, and tumour 3 is allocated in slice 74.

1) NEMA phantom data set: Feedforward neural network with one hidden layer has been used in this study. The training algorithm used with this network is the backpropagation algorithm. To evaluate the effect of neurons number in the hidden layer and achieve the best ANN performance for our application, different neurons numbers in

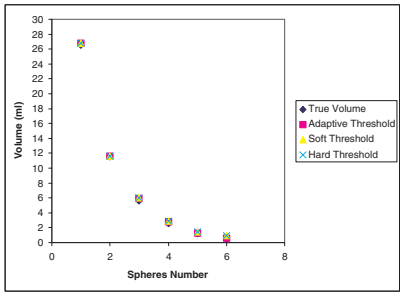

Fig. 2. The segmented volume for all spheres in NEMA data set using adaptive, soft, and hard threshold approaches respectively.

the hidden layer have been used. The maximum number of iteration used in the ANN is 1000 iterations. Hyperbolic tangent sigmoid transfer function "tan-sigmoid" has been used for all layers except the output layer where the linear activation function "purelin" is used. In this application 70% of the first data set have been used for training, 15% for validating, and 15% for testing.

The inputs features of the ANN have been extracted in spatial and wavelet domains. The utilised wavelet filter decomposes each slice from the input volume and produces four types of coefficients. The approximation coefficients, produced by HWT, represent most detailed information about the analysed slice, and the size of these coefficients (84 x 84) is half of the original size. A window of 12 x 12 voxels has been used to scan each input slice. The utilisation of this window has reduced the approximation coefficients size fed into the ANN each time without losing the slice details. It also reduced the required computational time. The ANN achieved good performance with very small mean squared error (MSE), $2.39e^{-16}$.

An objective evaluation for the artificial intelligence system outputs has been performed by comparing the sphere calculated volume with its true (original) volume. The experimental results have been repeated 10 times, and the average of the sphere volume measured using ANN is calculated. The calculated volume obtained from the ANN, and the percentage of the absolute relative error (ARE) for each sphere are presented in Table I. ANN has clearly detected all spheres, where spheres 1, 2, and 3 are accurately detected, spheres 4 is overestimated, and sphere 5 and 6 are underestimated. It worth mentioning that the proposed system has shown better performance compared to the thresholding and clustering based approaches which are used as ground truth. Adaptive, soft, and hard threshold approaches have been used to perform the segmentation. The best results obtained from these approaches is where adaptive threshold method is used, which is also used for the comparison with the other assessed techniques. Fig. 2 presents the obtained spheres volumes using three thresholding approaches. Table I illustrates a comparison between the assessed approaches in term of ARE. Thresholding approach has overestimated the volume of all spheres, while the exploitation of *K*-means clustering approach underestimates the volume of all spheres, particularly spheres 5, and 6.

During this study different number of neurons in the hidden layer have been used to validate the best design for the ANN, which is suitable for the proposed application. Levenberg-Marquardt back-propagation training algorithm has been used during the evaluation of neurons numbers in the hidden layer. Fig. 3 illustrates the effect of changing the number of neurons in the hidden layer on the training time at iteration 1000, performance using MSE, and regression respectively. The results obtained after this evaluation shows that the best number of the hidden neurons which corresponds to the smallest MSE, regression equal to 1, reasonable time, and good ANN outputs is 96 neurons. The segmented slices from thresholding, clustering and ANN in the wavelet domain are illustrated in Fig. 4.

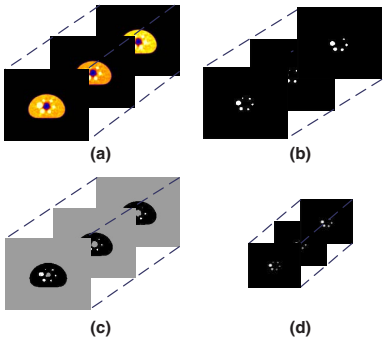

Fig. 4. NEMA Phantom data: (a) Original PET volume (168x168x66), (b) thresholded volume (168x168x66), (C) clustered volume (168x168x66), (d) segmented volume (84x84x66) from ANN and MRA.

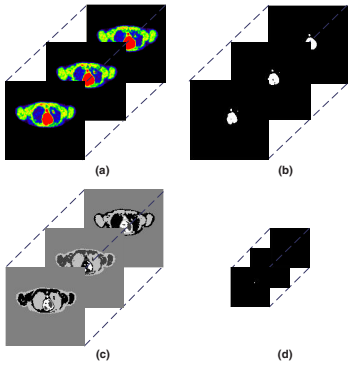

Fig. 5. Zubal Phantom data (Tumour 1): (a) Original PET volume (128x128x180), (b) thresholded volume (128x128x180), (C) clustered volume (128x128x180), (d) segmented volume (64x64x180) from ANN and MRA.

2) Zubal phantom data set: The proposed system was able to detect tumours in Zubal phantom data set with isotropic voxels. Tumour 1 with size 2 voxels was clearly detected in slice 68. Tumour 2 with size 3 voxels was also clearly detected in slice 57, and tumour 3 also clearly allocated in slice 74 with size 2 voxels. Due to space limit Fig. 5 shows just the segmented slices for tumour 1 from thresholding, clustering and ANN in the wavelet domain.

Similar segmented slices have been obtained using ANN in the spatial domain however more computational time and memory are required for all data sets in this domain.

B. Studying real PET volumes

The proposed approaches have been also tested on real PET volumes which contain lung tumour. A subjective evaluation based on the clinician knowledge has been carried out for the output of the proposed approaches. The tumour in these slices has a maximum diameter on the y-axis of 90 mm (estimated by histology). The segmented tumour using ANN in spatial and wavelet domains (after scaling) has a diameter of 90.098 mm. The segmented volumes using this system have clear detection of ROI as illustrated in Fig. 6.

C. Performance evaluation

In the field of AI a number of performance metrics can be employed to evaluate the performance of ANN. A confusion matrix (CM) is a visualization tool typically used in supervised and unsupervised learning approaches. The CM for NEMA data set shows that one voxel out of 65 ones in the segmented sphere 1 was misclassified. The two voxels of tumour 1 in Zubal data set were precisely classified

TABLE I
COMPARISON BETWEEN TRUE SPHERES VOLUMES, CALCULATED VOLUMES, AND ARE FOR THRESHOLDING, CLUSTERING AND ANN APPROACHES

Spheres		Thresholding		Clustering		ANN	
No.	True volume (ml)	Calculated volume (ml)	ARE (%)	Calculated volume (ml)	ARE (%)	Calculated volume (ml)	ARE (%)
1	26.52185	26.73747	0.81	25.73412	2.97	26.54335	0.08
2	11.49404	11.61763	1.07	11.00844	4.22	11.50635	0.10
3	5.57528	5.96411	6.97	5.27666	5.35	5.62866	0.95
4	2.57244	2.80616	9.08	2.39509	6.89	2.62730	2.13
5	1.15035	1.28824	11.98	1.03497	10.03	1.09806	4.54
6	0.52360	0.60613	15.76	0.46324	11.52	0.49280	5.88

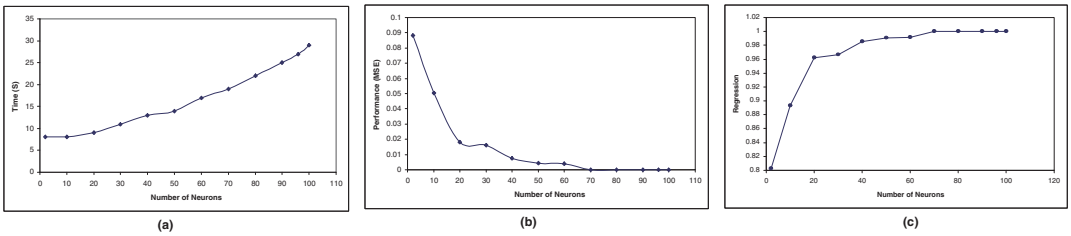

Fig. 3. Evaluating the number of neurons in the first hidden layer with (a) training time for 1000 iterations, (b) performance using MSE, (c) regression.

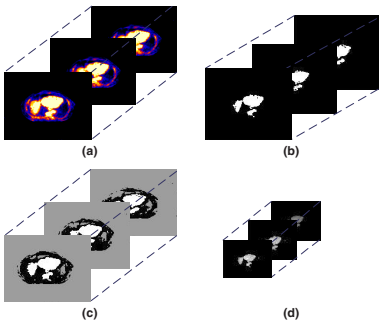

Fig. 6. Real PET data: (a) Original PET volume (128x128x178), (b) thresholded volume (128x128x178), (C) clustered volume (128x128x178), (d) segmented volume (64x64x178) from ANN and MRA.

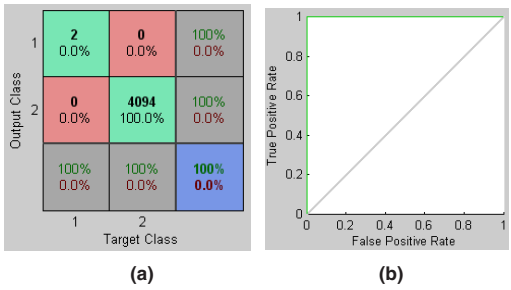

Fig. 7. Performance evaluation: (a) CM for Zubal phantom data, tumour 1, (b) ROC curve for Zubal phantom data.

as a first class and the remaining voxels (4094) classified in the other class. The other performance checking approach is receiver operating characteristic (ROC). This approach can be represented by plotting the fraction of true positives rate (TPR) versus the fraction of false positives rate (FPR), where the perfect point in the ROC curve is point (0,1). The curve for the NEMA data set is located near the perfect point and the FPR for the sphere voxels number is almost 0. Perfect ROC has been also obtained for Zubal data set and the FPR for tumour voxels number is 0. Due to the space limit Fig.7.a presents just CM for Zubal phantom data set, tumour 1, and Fig.7.b presents the ROC curve for this data set.

V. CONCLUSIONS AND FUTURE WORK

An objective and subjective evaluation for the intelligent system outputs have been carried out, CM and ROC are used to judge the ANN performance. The experimental results have shown a good performance for the ANN in detecting the tumours in spatial and wavelet domains for both phantom and real PET volumes. Ongoing research is focusing on the exploitation of other AI and feature extraction techniques.

REFERENCES

[1] D. A. Mankoff, M. Muzi, and H. Zaidi. *Quantitative analysis in nuclear oncologic imaging*. Springer, 2006.

[2] S. Basu. Selecting the optimal image segmentation strategy in the era of multitracer multimodality imaging: a critical step for imageguided radiation therapy. *Eur J Nucl Med Mol Imaging*, 36(2):180–181, 2009.

[3] S. Joo, W. K. Moon, and H. C.Kim. Computer-aided diagnosis of solid breast nodules on ultrasound with digital image processing and artificial neural network. *Proceedings of the 26th Annual International Conference of the IEEE EMBS*, 2004.

[4] K. Suzuki, H. Abe, H. MacMahon, and K. Doi. Image-processing technique for suppressing ribs in chest radiographs by means of massive training artificial neural network (MTANN). *IEEE Transactions on Medical Imaging*, 25(4):406–416, 2006.

[5] G. F. Luger. *Artificial intelligence : structures and strategies for complex problem solving*. Pearson Education Inc., 2009.

[6] P. K. Sahoo, S. Soltani, and A. K. C. Wong. A survey of thresholding techniques. *Comput. Vis. Graph. Image Proc*, 41:233–260, 1988.

[7] N. Otsu. A threshold selection method from gray-level histograms. *IEEE Transactions on Systems, Man, and Cybernetics*, 9(1):62–66, 1979.

[8] R. Gonzalez and R. Woods. *Digital Image Processing*. Prentice Hall, 2001.

[9] A. Amira, S. Chandrasekaran, D. Montgomery, and I. Uzun. A segmentation concept for positron emission tomography imaging using multiresolution analysis. *Neurocomputing*, 71:1954 – 1965, 2008.

[10] K. M. Rajpoot and N. M. Rajpoot. Hyperspectral colon tissue cell classification. *Proc. SPIE Medical Imaging*, 2004.

[11] A. K. Jain and R. C. Dubes. *Algorithms for Clustering Data*. Prentice Hall, 1988.

[12] Geneva University Hospital. *PET Instrumentation and Neuroimaging Lab*. 2009.